Ion-Exchanged Binuclear Ca_2O_X Clusters, $X = 1–4$, as Active Sites of Selective Oxidation Over MOR and FAU Zeolites

A. V. LARIN,[1] G. M. ZHIDOMIROV,[1,2] D. N. TRUBNIKOV,[1] D. P. VERCAUTEREN[3]
[1]*Department of Chemistry, MSU, GSP-2, Moscow 119992, Russia*
[2]*Boreskov Institute of Catalysis, Quantum Chemistry Department, SO RAN, Novosibirsk 630090, Russia*
[3]*Chemistry Department, University of Namur (FUNDP), Rue de Bruxelles 61, B-5000 Namur, Belgium*

Received 21 October 2008; Accepted 22 April 2009
DOI 10.1002/jcc.21340
Published online 4 June 2009 in Wiley InterScience (www.interscience.wiley.com).

Abstract: A new series of calcium oxide clusters Ca_2O_X ($X = 1–4$) at cationic positions of mordenite (MOR) and faujasite (FAU) is studied via the isolated cluster approach. Active oxide framework fragments are represented via 8-membered window (8R) in MOR, and two 6R and 4R windows (6R+4R) possessing one common Si—O—Si moiety in FAU. Structural similarities between the Ca_2O_X(8R) and Ca_2O_X(6R+4R) moieties are considered up to $X = 4$. High oxidation possibilities of the Ca_2O_2(*n*R) and Ca_2O_3(*n*R) systems are demonstrated relative to CO, whose oxidation over the Ca-exchanged zeolite forms is well studied experimentally. Relevance of the oxide cluster models with respect to trapping and desorption of singlet dioxygen is discussed.

 J Comput Chem 31: 421–430, 2010

Key words: zeolite; oxidation; isolated cluster approach; alkaline earth cations; singlet dioxygen; carbon monoxide

Introduction

Experimental data on desorption of singlet dioxygen from various cation exchanged forms of the mordenite (MOR) and faujasite (FAU) type zeolites have been accumulated in the last years.[1,2] To our knowledge, the work reported in ref. 2 is the first description of oxidation activity of ZnY (or ZnFAU) as compared to the oxidation properties of the FAU types with alkaline earth cations (Mg, Ca, Sr, Ba) that were already widely investigated earlier with respect to small alkenes,[3–5] toluene,[6,7] *p*-xylene,[8] cyclohexane,[7,9] propane,[10] and CO.[11–13] The usual accepted mechanism is a stabilization in the electric field (EF) of an "oxidized molecule—O_2" ion pair with an essential charge transfer.[3–7] However, the authors of ref. 10 met some contradictions between the low reaction yield for propane oxidation over BaY and the measured high EF. Moreover, weak interactions between the components of the ion pair complexes can hardly be the reason of the substantial shift in the energies of electronic transitions in oxidized organics.[3–7]

In a recent work, we proposed a new model for CO oxidation based on oxide Me_2O_X(8R) clusters (Me = Ca, Zn, $X = 1–3$) comparing the Ca- and Zn-exchanged forms of the MOR type (Si/Al = 3) zeolite.[14] The 8R symbol relates to the 8-membered ring (8R) window which opens the side pocket of the MOR main channel. Moderate activation barriers for the Me_2O_2(8R) cluster were evaluated for both Me cations, in agreement with high conversions of propylene oxidation over CaY and ZnY zeolites.[1]

The wide range of the MOR,[1,11,12] Y,[1–13] BETA,[8] ZSM-5,[8] and Linde (or A type)[13] zeolites, whose cationic forms are active in oxidation processes, suggests a secondary role of the framework in the oxidation. The stability of the Ca_2O_X clusters proposed in ref. 14 should hence be confirmed for other zeolite frameworks than MOR to demonstrate their possible formations in various different zeolite confinements. In the present work, we therefore compared the geometries of calcium oxide Ca_2O_X ($X = 1–4$) clusters at the cationic positions of MOR and FAU. Interestingly, we observed that the Ca_2O_X clusters could gradually change their activity with X, which deserves a separate study to select the most active oxidizing structure.

In this article, after a presentation of the computational strategy, we will discuss the relative energy and stability of the

Additional Supporting Information may be found in the online version of this article.

Correspondence to: A. V. Larin; e-mail: nasgo@yandex.ru

Contract/grant sponsors: FUNDP (iSCF center), FNRS-FRFC, Loterie Nationale; contract/grant number: 2.4578.02

Contract/grant sponsor: CGRI; contract/grant number: convention 2008/18342

Ca_2O_X (X = 1–4) clusters. Additionally, we will compare the differences between the optimized Ca_2O_X geometries for the different MOR and FAU frameworks. For both zeolite types, we will compare the activation barriers for CO oxidation over the Ca_2O_2 and Ca_2O_3 clusters.

Computational Details

Mordenite

The geometry of a supercell with two primitive cells of Zn-form of MOR with Al in the position T4[15] on the opposite sides of the large channel was fully optimized using the GULP code[16] and Catlow force field (FF).[17,18] One of the 8R windows which opens the side pockets in ZnMOR was isolated from the 3D structure and the second Si atom was replaced by Al at T4 (Fig. 1, top). Keeping the Zn cation near the 8R window and capping the ruptured T—O bonds of all T atoms (T = Si, Al) by H atoms, one reached a neutral fragment $ZnAl_2Si_6O_8H_{16}$ in which one replaced Zn by Ca (Fig. 1, top). The T—H lengths were further optimized using GAUSSIAN03[19] at the B3LYP/6-31G* level with fixed O—T—H and T′—O—T—H angles and fixed positions of the other atoms. Then, H atoms only were fixed and the coordinates of the other atoms were varied. A second basis set (denoted below as *ps* case) combining 6-31G* for all the atoms and LANL2DZ* for the Ca cations was also applied. The similarity of the geometries obtained with the two bases was already illustrated for Ca_2O_X(8R).[14] To determine the reaction coordinate for CO oxidation, we applied the QST3 algorithm as supplied with GAUSSIAN03.[19] The heat of CO oxidation was also calculated at the MP2/6-31G* level over Ca_2O_X(8R) because of the smaller dimension of the atomic orbital space relative to the one of Ca_2O_X(6R+4R).

An important step was then to check the influence of the spatial restraints on the resulting geometry and energy for a larger fragment $CaAl_2Si_6O_{24}H_{16}$, obtained by the addition of a layer of 16 O atoms to the 8R window T atoms, thus replacing the capping hydrogens. To add the oxygens, the optimized small cluster was embedded in the initial crystallographic position. It was achieved via a series of rotations of the small cluster as a whole, i.e., with fixed relative optimized coordinates in order to reach minimal distances between the O in crystallographic positions and the optimized H. The already optimized hydrogens were replaced by the nearest oxygens in crystallographic positions while additional H atoms were added to the new O atoms in the direction of the nearest T atoms. Then, the optimization procedure of the H coordinates was repeated as for the smaller cluster.

Faujasite

For FAU, we repeated the same procedure as used for MOR but starting from the $Na_2Al_2Si_6O_9H_{14}$ fragment of the X-ray diffraction (XRD) model of the NaFAU zeolite (Si/Al = 3) including 6R and 4R windows[20] (Fig. 1, bottom). The Na cations, corresponding to the II and III types, were then replaced by Ca cations. No extended cluster with an extra layer of O atoms was constructed like for MOR.

Optimization of Cationic Positions

The optimization of the ZnMOR form was first performed at the FF empirical level considering periodic conditions with the GULP code. For CaY, we started using the initial XRD NaY model.[20] Taking into account the ZnMOR and NaY fragments to study the Ca cationic form can be done if the substituting cation does not distort specifically the lattice. In this sense, the analysis of literature data reveals about no specific distortion related to the Zn, Na, and Ca cationic forms. Only small possible differences between the Zn- and Ca-forms of MOR could be suggested indirectly, as shown by the comparison of the lattice constants for Na(50%)Ca(50%)Y[21] and ZnY.[22] For these models, the lattice constant of NaCaY is 24.74 Å (Si/Al = 2.33[21]). The lattice constant of ZnY (Si/Al = 2.37) varies from 24.68 Å for Na(45%)Zn(55%)Y to 24.75 Å for Na(26%)Zn(74%)Y.[22]

Differences between the geometries of the Na- and Ca-forms of FAU come from the smaller size of the Na cation whose replacement by the larger Ca cation can change the structure of the lattice. The variations of the lattice constants while replacing Na by Ca are however rather small so that they, for example, were neglected in ref. 20. This last suggestion can be supported by the closeness between the lattice constants of NaA and CaA (Linde LTA forms), i.e., 12.30 ± 0.02 Å for NaA and 12.25 ± 0.02 Å for CaA using the spatial *Pm3m* group for the XRD fitting.[23] These comparisons from literature[20–23] thus confirm the smallness of the lattice perturbations while exchanging the cation and justify the application of either the initial FF optimized ZnMOR model or the XRD NaY model to further optimize the isolated cluster Ca-model at the quantum mechanical level.

Results

Relative Stabilities and Geometries of the Ca_2O_X(nR) Clusters

The optimized structures of the Ca_2O_X(8R) in MOR and Ca_2O_X(6R+4R) in FAU clusters (X = 1–4) are presented in Figure 2. Several geometrical parameters are shortly described in Tables 1 and 2. The stability of the clusters was evaluated according to the consequent oxidation by oxygen in triplet state:

$$Ca_2O_{X-1}(n\mathrm{R}) + \frac{1}{2}O_2 \rightarrow Ca_2O_X(n\mathrm{R}) \quad (1)$$

with $X \geq 2$. All the formation steps of the upper oxides, i.e., $X > 2$, were estimated as exothermic for the 6R+4R FAU fragment (Table 1). For all X values, we observed a slightly larger heat of formation for FAU than for MOR. With the exception of Ca_2O_4, the Ca...Ca distance in all cases is larger for the 6R+4R cluster in FAU as compared to the one for the 8R

The application of the LANL2DZ basis set will be important in future studies for heavier alkaline earth cations like Sr and Ba for which no 6-31G basis set has been developed so far.

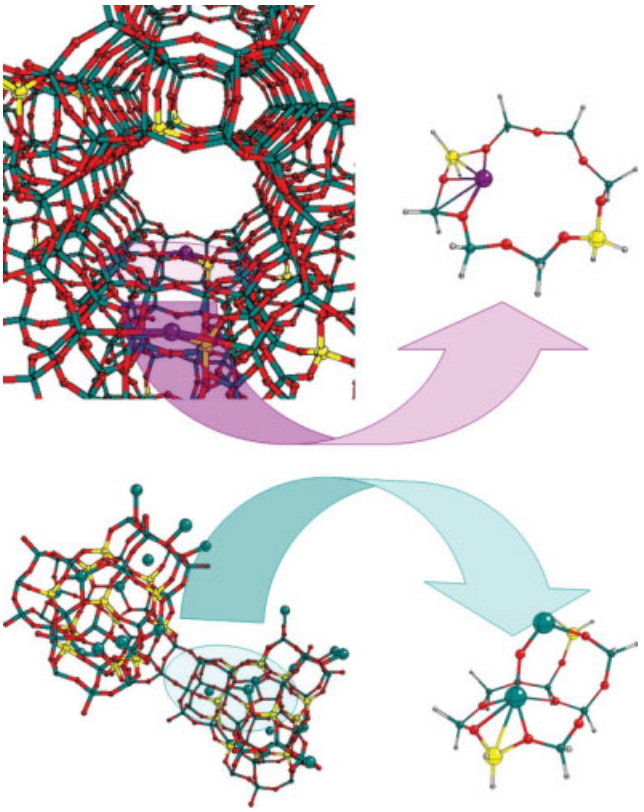

Figure 1. Selection of the chosen fragments from ZnMOR (top) and NaFAU (bottom). The color code is as follows: Zn in purple, Na in green (larger spheres), O in red, Si in green (smaller spheres), Al in yellow, and H in gray.

cluster in MOR. This shorter distance can be the reason of the lower stability of the Ca_2O_X(8R) model versus the one of Ca_2O_X(6R+4R), for all X values, with the exception of $X = 1$.

Upon gradual decrease of the absolute heat of Ca_2O_X formation with X, the Ca_2O_4(8R) form in MOR is not allowed thermodynamically; reaction (1) is endothermic: 5.2 kcal/mol for $X = 4$ (Table 1). This cannot be a result of the spatial hindrance of the Ca_2O_4(8R) complex because of the larger Ca···Ca distance of 3.940 Å relative to the one of 3.913 Å in Ca_2O_4(6R+4R), whose formation is exothermic: −1.7 kcal/mol for reaction (1) when $X = 4$ (Table 1). However, a minor exothermic effect by −1.1 kcal/mol is calculated in MOR at the B3LYP/6-31G* level for the $Ca_2O_2+O_2$ reaction. We can thus confirm a dependence of the heat of Ca_2O_4(nR) formation versus the zeolite type.

Ca_2O_4(nR) Moieties

To the best of our knowledge, the existence of a Ca_2O_4(nR) moiety has never been shown before. Stable geometries for the Ca_2O_4 cluster were found here for both 8R in MOR and 6R+4R in FAU fragments (Figs. 2d and 2h). The O_4 moiety presents a plain trapezium form based on two sides of O_2 molecules with bond lengths of 1.359 and 1.360 Å in MOR, and 1.358 and 1.362 Å in FAU, strongly elongated versus the experimental gas value r_e = 1.201 Å[24] or theoretical 1.214 Å obtained at the B3LYP/6-31G* level. The lengths of the parallel sides of the trapezium equal 1.998 and 2.498 Å for MOR, and 1.928 and 2.514 Å for FAU. For MOR, the O—O axes are located nearly in a same plane approximately perpendicular to the Ca···Ca axis. The plane is slightly shifted toward Ca2 resulting in an average

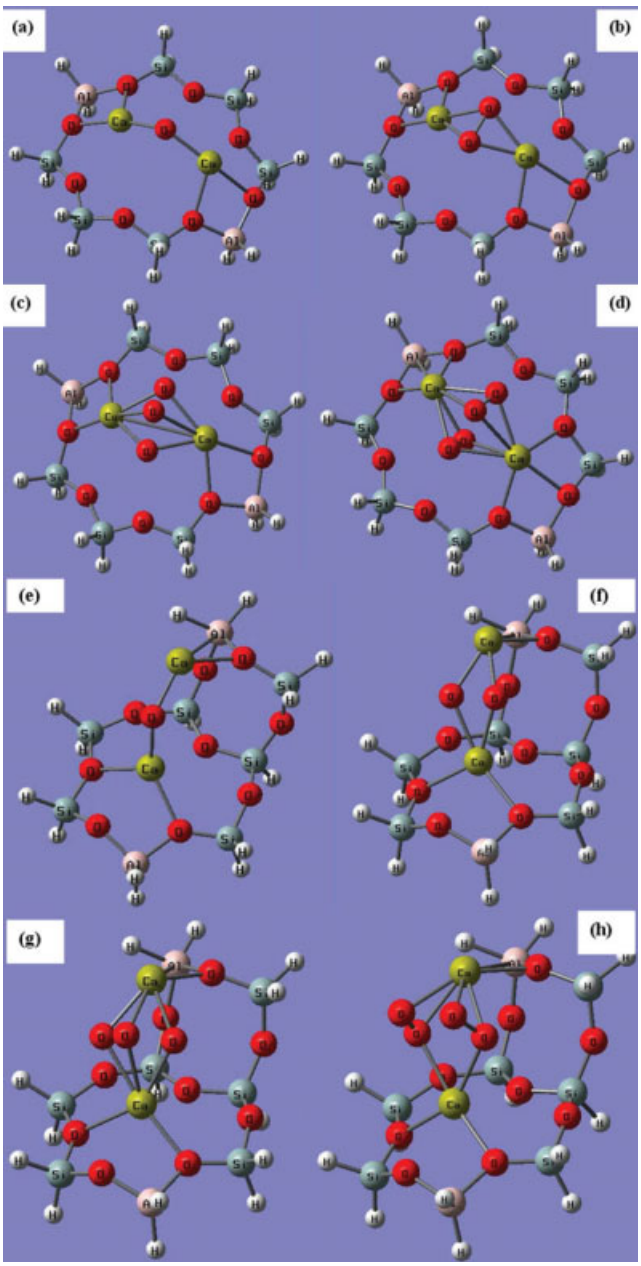

Figure 2. Optimized structures of the small Ca_2O_X(nR) clusters, for 8R in MOR (a–d) and 6R+4R in FAU (e–h): $X = 1$ (a, e), $X = 2$ (b, f), $X = 3$ (c, g), $X = 4$ (d, h), calculated at the B3LYP/6-31G* level. Atomic labels of Figure 2 are used in Table 2. The color code is as follows: O in red, Si in blue, Al in pink, H in white, and Ca in yellow.

Table 1. Relative ΔU (kcal/mol) and Total U (a.u.) Energies of the Ca_2O_X(8R) in MOR and Ca_2O_X(6R+4R) in FAU Formation for X = 2–4 at Singlet States According to Reaction (1), Ca···Ca and O—O Distances (Å), Calculated at the B3LYP/6-31G* Level.

	$\Delta U/U$		Ca. . .Ca		O—O	
X	8R	6R+4R	8R	6R+4R	8R	6R+4R
1	−/−4264.491843, −/−4257.092215[a]	−/−4264.491843	3.746	3.946	–	–
2	−24.8/−4339.689680, −27.9/−4332.108661[a]	−26.5/−4413.862290	3.754	3.904	1.556	1.572
3	−6.1/−4414.857819, −12.7/−4407.090918[a]	−8.6/−4489.034256	3.661	3.801	1.493, 1.495	1.496, 1.498
4	5.2[b]/−4490.007960	−1.7/−4564.195254	3.940	3.913	1.340, 1.359, 1.998, 2.498	1.358, 1.362, 1.928, 2.514

Negative ΔU values of reaction (1) correspond to an exothermic effect. Total electronic energy of O_2 is −150.316605 a.u. at the B3LYP/6-31G* level.

[a]At the MP2/6-31G* level; total electronic energy of O_2 is −149.944087 a.u.

[b]Slight exothermic effect of −1.1 kcal/mol is observed according to the Ca_2O_2(8R) + O_2 → Ca_2O_4(8R) formation.

difference between the Ca1—O and Ca2—O distances of 0.03–0.06 Å (Fig. 2d). For FAU, the shift of the O_4 plane toward the upper Ca cation is similar for the two lower O atoms, i.e., 0.03–0.07 Å, but more emphasized, i.e., 0.8–0.9 Å, for the two upper O atoms (Fig. 2h). Distances of 1.998 and 1.928 Å of the central O—O bond, i.e., upper parallel side of the O_4 trapezium for 8R and 6R+4R, respectively (Table 1), are smaller than the sum of the covalent or ionic radii for O, i.e., 1.21 and 1.35 Å, or even more.[25] This length allows discussing unusual O—O—O—O chains stabilized in the zeolite space. Characteristic vibrations of the Ca_2O_4(8R) at 1129, 556, and 432 cm^{-1} computed at the B3LYP/6-31G* level also clearly manifest a unique group Ca_2O_4 and not two separate O_2 species with the frequency of 1657 cm^{-1} at the same B3LYP/6-31G* level.

Different Ca Bonding in MOR and FAU

The geometries of the Ca_2O_X(8R) clusters (X = 1–3) were already discussed in ref. 14. Here, we include Ca_2O_4(nR) that was not yet described. Several main geometrical parameters for X = 1–4 are compared in Tables 1 and 2. The Ca—O bond lengths in the Ca_2O_X(nR) clusters vary in close ranges for a same X value; the average Ca—O distance with the oxygens of the O_X group increases with X (Table 2). Regarding the bonds between Ca and the framework O_f oxygens, a qualitative difference appears between MOR and FAU. For MOR, the Ca···O_f bond lengths are relatively similar, while in FAU they are not. For MOR, the Ca1···O_f and Ca2···O_f bond distances in Ca_2O(8R) are close, i.e., 2.354, 2.449, and 2.501 Å for Ca1···O_f and 2.320 and 2.387 Å for Ca2···O_f (Fig. 2a, values not shown in Tables). With the expansion of Ca_2O(8R), i.e., addition of 16 O atoms, slightly longer distances are obtained for the Ca1···O_f bonds, i.e., 2.435, 2.399, and 2.721 Å, while the Ca2···O_f distances either shorten or elongate, i.e., 2.438 or 2.374 Å, respectively. The values thus vary slightly less than 0.05 Å with X. As a result of the closeness between the Ca1···O_f and Ca2···O_f bond lengths in the 8R model, the difference between the Ca atomic charges does not exceed 0.01–0.05 e^-, for any X value (Table 2). The charge difference between Ca1 and Ca2 decreases with X owing to a larger influence of the framework O atoms.

Table 2. Mulliken Charges $Q_0^0(e^-)$, Bond Lengths (Å), and Bond Angles (°) Between Ca Atoms and O Atoms of the O_X Group for Ca_2O_X(8R) in MOR and Ca_2O_X(6R+4R) in FAU Calculated at the B3LYP/6-31G* Level.

	Q_0^0(Ca1), Q_0^0(Ca2)		Ca—O—Ca		Ca—O	
X	8R	6R+4R	8R	6R+4R	8R	6R+4R
1	0.913, 0.954	0.777, 0.987	124.48	137.35	2.115, 2.118	2.089, 2.147
2	1.069, 1.099	0.910, 1.144	111.27, 111.74	121.4, 121.2	2.244, 2.245, 2.247, 2.236	2.200, 2.275, 2.206, 2.275
3	1.090, 1.122	0.916, 1.163	103.82, 94.16, 103.96	108.99, 102.37, 109.40	2.312, 2.513, 2.324, 2.336, 2.484, 2.328	2.374, 2.294, 2.503, 2.374, 2.377, 2.280
4	1.145, 1.157	0.949, 1.153	108.33, 100.79, 121.15, 109.38	111.81, 89.13, 111.72, 89.04	2.442, 2.583, 2.274, 2.445, 2.417, 2.530, 2.249, 2.382	2.383, 2.401, 3.142[a], 3.150[a], 2.345, 2.381, 2.327, 2.375

[a]The bond is not shown in Figure 2h.

Table 3. Natural Bond Orbital (NBO) and Mulliken (Mull.) Charges (e^-) of the Ca_2O_X(8R) Clusters (X = 1–3) Calculated at the B3LYP/6-31G* Level.

	Ca_2O		Ca_2O_2		Ca_2O_3	
Atom	NBO	Mull.	NBO	Mull.	NBO	Mull.
Ca1	1.793	0.913	1.857	1.069	1.853	1.090
Ca2	1.797	0.954	1.859	1.099	1.853	1.122
Al6	1.399	0.563	1.400	0.562	1.400	0.566
Al12	1.397	0.607	1.399	0.602	1.400	0.605
O8	−1.351	−0.778	−1.355	−0.780	−1.358	−0.780
O9	−1.359	−0.765	−1.362	−0.778	−1.362	−0.778
O15	−1.364	−0.787	−1.368	−0.789	−1.370	−0.789
O18	−1.347	−0.740	−1.348	−0.744	−1.347	−0.744
O19	−1.648	−0.898	−0.894	−0.580	−0.785[a]	−0.519[a]
O20	–	–	−0.897	−0.584	−0.790[a]	−0.527[a]
O21	–	–	–	–	−0.217[b]	−0.175[b]

All atomic positions correspond to Figure 4, except for the O20 and O21 atoms of the Ca_2O_X group.
[a]Side atom of the O_3 group.
[b]Central atom of the O_3 group.

On the other hand, the Ca1···O_f and Ca2···O_f bond lengths are substantially different in FAU. The charge of the lower Ca1 is usually smaller by approximately 0.2 e^- than the one of the upper Ca2 (Figs. 2e–2h). Because of the weaker bonding of Ca2 toward the framework oxygens, the O_X group is usually slightly closer to it. The bond lengths between the Ca atoms and the framework oxygens, i.e., short Ca1···O_f distances of 2.360, 2.481, and 2.670 Å, and one unique Ca2···O_f distance of 2.364 Å in Ca_2O(6R+4R), vary little with X (not shown in Tables). The closer location of the O_X group to Ca2 for Ca_2O_X(6R+4R) in FAU, notably, allows to separate the CaO_X group which could be formally considered as an inclusion to the Ca-exchanged neutral form. The sum of the atomic Mulliken charges of the atoms of the CaO_X group decreases from 0.077 e^- to −0.031, −0.540, and −0.103 e^- while varying from X = 1 to 4, respectively.

Mulliken and Natural Bond Orbitals Charges

The Mulliken charges for the Ca_2O_X(8R) clusters (X = 1–3) were compared to the charges obtained with the natural bond orbitals (NBO) analyses[26] as adopted in GAUSSIAN. Most of the framework NBO charges, i.e., for both Al atoms, and the O8, O9, O15, O18 atoms close to Ca and Al, are twice as much larger than the respective Mulliken charges (Table 3). However, the relative charge values for the same atoms mainly coincide for both NBO and Mulliken types, i.e., O15 and O18 have the largest and smallest charges in absolute value between the framework O atoms which coordinate the Ca cations for both NBO and Mulliken schemes. The smaller the charges, the smaller the difference between the NBO and Mulliken O charges in the binuclear cluster, i.e., for the O19, O20, O21 atoms of the O_3 group. The small O21 absolute values considering both NBO (−0.217 e^-) and Mulliken (−0.175 e^-) schemes deserve some particular attention. Such a kind of electrophilic O atom could be the object of further testing of the high catalytic activity.

We should also note the similarity of both NBO or Mulliken charges of the framework atoms between the Ca_2O(8R), Ca_2O_2(8R), and Ca_2O_3(8R) clusters. The charges of the atoms for the Ca_2O_X group nearly coincide between X = 2 and 3, while they differ versus those for the smallest Ca_2O group. The similarity between the NBO and Mulliken Q_0^0(Ca)/Q_0^0(O) ratio, the O atom belonging to the binuclear Ca_2O_X cluster, should be denoted for any X values. For example, NBO and Mulliken ratios of Q_0^0(Ca1)/Q_0^0(O19) are 1.09 and 1.02, 2.08 and 1.84, 2.36 and 2.10 for X = 1, 2, and 3, respectively (Table 3). It signifies that the NBO and Mulliken schemes provide similar relative atomic charges while the absolute NBO charge values are larger.

Singlet Dioxygen

Zeolite structures which could trap and produce singlet dioxygen have been the topic of long experimental research.[1,2] The binuclear Ca_2O_X(nR) clusters at cationic positions studied herein are perspective candidates for producing singlet O_2. For all X values from 1 to 4, we checked the stability of the cluster singlet states versus the triplet ones for both cluster types in MOR and FAU (Table 4). In all cases, the singlet states are more stable than the triplet ones at the B3LYP levels for MOR and FAU, and MP2 level for MOR, when SCF convergence was achieved. MP2 computations provided an even much higher stability for the singlet Ca_2O(8R) and Ca_2O_2(8R) clusters with the same basis set. For comparison of the data in Table 4 with O_2 in the gas state, the triplet state of O_2 gains 31.3 kcal/mol versus the singlet one, irrespective if full or frozen core MP2 calculations are considered.

The formation of singlet O_2 is thus straightforward from Ca_2O_X(nR), i.e., non spin forbidden, because the remaining Ca_2O_{X-2}(nR) part is also singlet. While desorbing from the ground singlet state of Ca_2O_X(nR), a part of O_2 could change its multiplicity to the most stable ground triplet O_2, while at least the other O_2 part keeps it as approved by the experimental studies.[1,2] It seems that the main part of molecular oxygen turns out to be desorbed in triplet O_2 state, i.e., two desorption peaks for triplet O_2 were evaluated with a concentration of 10^{18} and 10^{15} molecule/cm^3 from FAU and as 10^{17} and 10^{15} molecule/cm^3

Table 4. Relative Energies (kcal/mol) Between the Singlet (S = 0) and Triplet (S = 1) States Calculated at the B3LYP/6-31G* Level for the Ca_2O_X(8R) Clusters in MOR and Ca_2O_X(6R+4R) Clusters in FAU.

X	8R	6R+4R
1	55.8, 118.0[a]	42.7
2	31.2, 41.9[a]	–[b]
3	14.2	12.2
4	–[b]	10.1

Positive values correspond to high singlet stability.
[a]At the MP2/6-31G* level.
[b]No SCF convergence for S = 1.

from MOR in air and helium flows, respectively, versus approximately 10^{13} molecule/cm^3 for singlet O_2 within both zeolites. Such small concentration, i.e., 10^{13} molecule/cm^3 suggested possible modifications of the reactive centers by singlet O_2 in zeolites.[2]

The $Ca_2O_2(n\mathrm{R})$, $Ca_2O_3(n\mathrm{R})$, and $Ca_2O_4(n\mathrm{R})$ moieties can be the source of singlet O_2. Its production from $Ca_2O(n\mathrm{R})$ seems to be forbidden because of the formation of a nonstable structure. The small or even positive heat of $Ca_2O_4(n\mathrm{R})$ formation (Table 1) shows the most probable role of the $Ca_2O_2(n\mathrm{R})$ and $Ca_2O_3(n\mathrm{R})$ clusters.

Oxidation in Mordenite

The oxidation activity of alkaline earth zeolites reported in refs. 1–12 was analyzed by us here for CO oxidation over both $Ca_2O_2(8\mathrm{R})$ and $Ca_2O_3(8\mathrm{R})$ clusters (Table 5). At both basis set levels, i.e., 6-31G* and *ps*, we observed close computed activation barriers of the reactions but very different heats of the reactions.

$Ca_2O_2(8R)$

$Ca_2O_2(8\mathrm{R})$ in MOR holds its geometry in the reaction complex (Fig. 3a), which explains the moderate heat of adsorption for physisorbed CO (Table 5). The reaction coordinate corresponds to the vibrations of CO towards one O atom of the Ca_2O_2 group. This motion is easily partitioned due to the large reduced mass, i.e., 14 a.m.u., versus other 15 imaginary frequencies whose reduced masses range between 1 and 9 a.m.u. and describe the freedom degrees of the fixed H atoms. The largest vector displacements around 0.3–0.6 Å correspond to the C and O atoms of the CO molecule and to the O atoms of the Ca_2O_X group. The largest displacements of the other atoms are below 0.05 Å for the Ca cations and even smaller for the other ions. Imaginary frequencies calculated at the B3LYP/6-31G* level along the reaction coordinates were 673.7*i*, 695.0*i*, and 750.3*i* cm^{-1} for the —Al—O—(Si—O)$_m$—Al— (m = 1–3) 8R window, respectively. The relatively large drop of imaginary frequency from 750.3*i* to 669.2*i* cm^{-1} corresponds to the replacement of the 6-31G*(Ca) cation basis set by the LANL2DZ(Ca) one for the favored case of m = 3. Different numbers of 13 or 16 imaginary frequencies were calculated for each m case that correspond to fixed freedom degrees of 16 fixed H atoms. The reaction coordinate for the transition state corresponds to the vibrations of CO toward one O atom at the $Ca_2O_2(8\mathrm{R})$ cluster (shown in Supporting Information). The computations with the large model (Fig. 4) slightly shift both the activation barrier, i.e., 33.2 kcal/mol instead of 35.7 kcal/mol (Table 5), and result in minor changes of the cluster geometry.

Minor variations of the heats of oxidation reactions in the framework of the large cluster model relative to the ones in the small model allows to conclude in a sufficiently accurate estimation of the structural relaxation with the larger model. The increase of the cluster is however not enough to properly calculate the electrostatic potential (EP) and its derivatives which can be important for modeling of chemical processes in bivalent cation exchanged zeolite form. Even if the short range part of the EP and EF produced by the cluster containing two close cations can be large, the "cluster" EP and EF values do not correspond to their convergent values relative to possible expansion of the surrounding atoms involved into calculation of electrostatic properties. Let us add that we are currently addressing to the cumulative coordinate (CC) method[27,28] in order to model the EP and the EF. The CC method indeed allows a parametrization of the charges and atomic multipole moments of the atoms of the remote part of the system that needs to be considered within the QM/MM method.

Table 5. $\Delta E^{\#}$ Activation Barriers of the $Ca_2O_X(8\mathrm{R})$ + CO → $Ca_2CO_{X+1}(8\mathrm{R})$ Oxidation Reaction, ΔE_{CO} Heat of CO Adsorption, ΔU Heat of Oxidation Reaction, and ΔE_{CO2} Heat of CO_2 Adsorption, on Small (S) or Large (L) $Ca_2O_X(8\mathrm{R})$ Clusters of MOR Calculated at the B3LYP Level and 6-31G* Basis Sets for all Framework Atoms, and 6-31G* or LANL2DZ (*ps*) for Ca Cations.

Energy Values	X = 2			X = 3	
	S/ps	S/6-31G*	L/6-31G*	S/ps	S/6-31G*
$\Delta E^{\#}$	31.5	35.7	33.2	29.4	32.4, 19.7[a]
ΔE_{CO}	12.7	13.4	13.0	11.5	12.4, 15.1[b]
ΔU	108.1	106.9	108.2	73.5	72.3, 78.9[a], 68.9[b]
ΔE_{CO2}	74.4	74.5	75.1	22.4	20.4, 25.7[b]

All values are in kcal/mol.
[a]At the PW91PW91/6-31G* level.
[b]At the MP2/6-31G* level.

A comparison of the initial (Fig. 3) with the optimized small cluster models reveals the minor distortion of the 8R window. This *a priori* confirms the accuracy of the chosen isolated cluster model with respect to the zeolite framework. However, earlier works showed a possible relaxation of the more remote layers around the reactive center.[29] Hence, an extension of the cluster is required for complete relaxation of the system.

Detailed analyses of the geometrical parameter and atomic charge variations for the CO and cluster atoms were performed for the three steps of the CO oxidation (Table 6). The comparison of the bond lengths reveals a slight shortening of the Al—O and Si—O bonds, around 0.03–0.04 Å and 0.01–0.02 Å, respectively. Variations of the Si—O—Al angles do not exceed 1 degree. The small window relaxation seems to correlate with the small structural changes for the adsorption complex. The maximal variation of the torsional Ca—O—O—Ca angle is 5.5°, while the Ca—O bonds vary by less than 0.01–0.02 Å, with the exception of 0.06 Å for the Ca1—O18 case.

It is interesting to trace the charge redistribution of the CO···$Ca_2O_2(8\mathrm{R})$ reactive part along the REA → TS → PRO sequence (Table 6). Here below, we will consider the values related to the large model as the most accurate one, even though the difference versus the data for the small model is indeed minor. The total charge of the two Ca cations rises by 0.074 e^- between the large models of TS and PRO cases, while the total charge of CO and the two O19 and O20 atoms which forms together the $CO_3^{\delta-}$ ion decreases by 0.088 e^-, respectively. Absolute values of the O charges rise from the REA to the PRO stages, i.e., by 0.4 e^- for O22. However, the total charge δ of

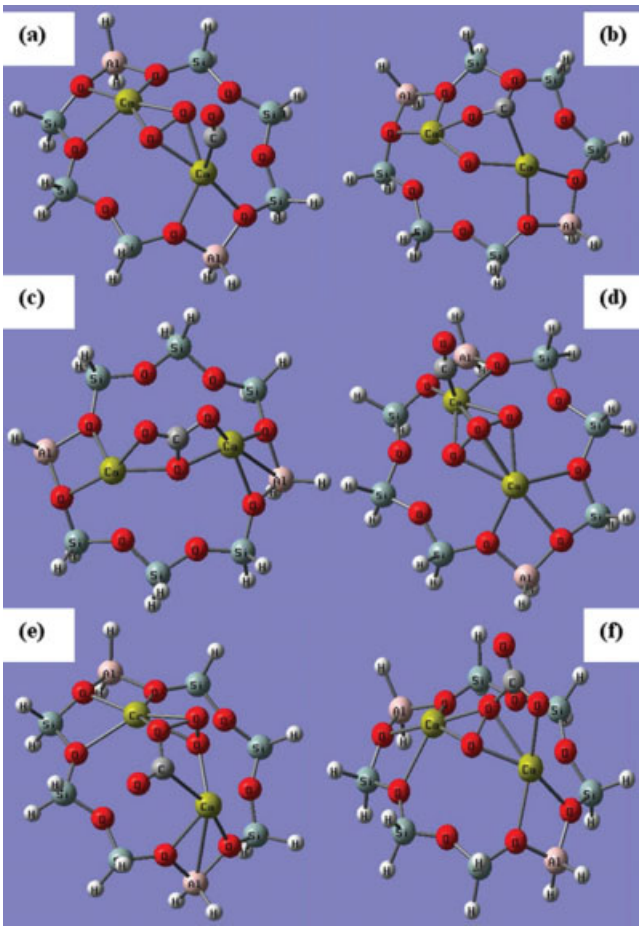

Figure 3. Optimized structures of the reagent (a, d), transition state (b, e), and product clusters (c, f) for CO oxidation over the small $Ca_2O_X(8R)$ clusters in MOR calculated at the B3LYP/6-31G* level, for $X = 2$ (a–c) and $X = 3$ (d–f). The color code corresponds to the one of Figure 2; C in gray.

the $CO_3^{\delta-}$ ion is -1.099, -1.090, and -1.178 e^- for the REA, TS, and PRO stages, respectively, with the large model. The total charge of the two Ca cations also varies very few, i.e., 2.069, 2.022, and 2.096 e^- at the REA, TS, and PRO reaction steps. Even if the more essential charge variation of Ca2 takes place in the same sequence, i.e., 0.958, 1.027, and 1.090 e^-, its bond lengths and angles change very little relative to the ones of Ca1. These minor variations of the total charge of the CO...Ca_2O_2 group between the reaction steps suggest a moderate or small influence of the EP on the stabilization of the TS relative to the stabilization of the reagents and products. However, the redistribution of the charge values over the O atoms signifies a possible effect of the EF and its gradient, of lower order of value than the usual stabilization effect due to the EP.

$Ca_2O_3(8R)$

The favored TS geometry for the reaction CO...$Ca_2O_3(8R)$ complex in MOR corresponds to the CO coordination near Ca (Fig. 3e), as for the $Ca_2O_2(8R)$ cluster (Fig. 3b). The most intriguing part, while searching the reaction coordinate for CO oxidation over $Ca_2O_3(8R)$, was the choice between either the extreme or the central O atom of the Ca_2O_3 group to form CO_2. Such problem was indeed not encountered for $Ca_2O_2(8R)$ with two oxygens in approximately symmetric positions. Finally, either of the two extreme O atoms of the O_3 group can be involved into the CO_2 formation. The TS geometry turns out to be very similar to the case of CO oxidation over $Ca_2O_2(8R)$. The reaction coordinate corresponds to the vibrations of CO and one O atom as observed for the TS at the $Ca_2O_2(8R)$ cluster. Respective imaginary frequencies of $695.2i$ or $678.4i$ cm^{-1} were calculated using B3LYP with the 6-31G* or *ps* basis sets at the Ca cation position in the 8R ring with —Al—O—(Si—O)$_3$—Al— alternation. The difference can be considered as minor.

The main differences between $Ca_2O_2(8R)$ and $Ca_2O_3(8R)$ in the course of oxidation are related to the heat of reaction and heat of CO_2 adsorption which are much larger for $Ca_2O_2(8R)$. We assigned this increase to the strong bidentate CO_2 chemisorption over $Ca_2O_2(8R)$ resulting in the CO_3^{2-} anion (Fig. 3c). Spatial restrictions do not allow the same CO_2 coordination for $Ca_2O_3(8R)$ (Fig. 3f). These observations reveal the different heats of CO_2 desorption for each reaction step. Respective $\Delta E^{\#}$, ΔE_{CO}, ΔE_{CO2}, and ΔU variations (Table 5) follow the same trends as observed for CO oxidation over $Ca_2O_2(8R)$ (Table 5). MP2 computations confirm the ΔE_{CO}, ΔE_{CO2}, and ΔU values with the same basis set (Table 5).

Oxidation in Faujasite

The data for the CO oxidation over two ($X = 2$ and 3) complexes in CaFAU are presented together due to their similarities relative to the data obtained for the $Ca_2O_X(8R)$ of CaMOR. A

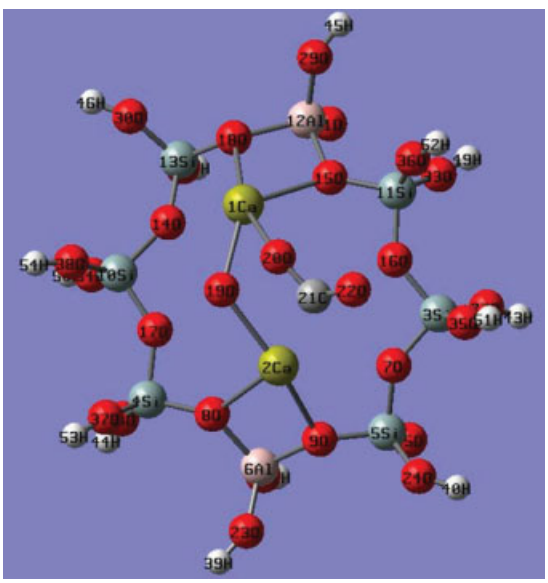

Figure 4. Optimized structure of the extended cluster for the transition state complexes for CO oxidation over $Ca_2O_2(8R)$ in MOR calculated at the B3LYP/6-31G* level. The color code corresponds to the one of Figure 3. Atomic labels of Figure 4 are used in Table 6.

Table 6. Mulliken Atomic Charges Q_0^0 (e^-) and Geometrical Parameters of the Reagents (REA), Transition States (TS), and Products (PRO) of CO Oxidation Reaction Over the Small and Large Ca_2O_2(8R) Complex of the MOR Type (Distances in Å, Angles in Degrees) Calculated at the B3LYP/6-31G* Level.

	REA		TS		PRO	
Parameter	Large	Small	Large	Small	Large	Small
Q_0^0(Ca1)	1.101	1.114	0.995	1.021	1.036	1.058
Q_0^0(Ca2)	0.958	0.965	1.027	1.033	1.090	1.088
Q_0^0(O19)	−0.567	−0.572	−0.594	−0.601	−0.632	−0.629
Q_0^0(O20)	−0.569	−0.575	−0.363	−0.361	−0.755	−0.768
Q_0^0(C21)	0.280	0.278	0.349	0.338	0.839	0.854
Q_0^0(O22)	−0.243	−0.220	−0.482	−0.460	−0.630	−0.631
Ca2−O9	2.349	2.368	2.318	2.338	2.300	2.300
Ca2−C21	2.686	2.695	2.665	2.629	2.692	2.687
Ca2−O8	2.397	2.394	2.437	2.414	2.420	2.408
Ca2−O19	2.265	2.254	2.251	2.252	3.814	3.923
Ca2−O20	2.274	2.268	2.964	2.970	2.259	2.259
Ca2−Ca1	3.671	3.754	3.847	3.936	4.195	4.302
O19−O20	1.552	1.556	1.857	1.851	2.237	2.239
Ca1−O20	2.263	2.258	2.428	2.405	2.253	2.259
Ca1−O19	2.263	2.252	2.216	2.217	2.376	2.348
C21−O20	2.702	2.781	1.297	1.304	1.359	1.363
C21−O22	1.139	1.136	1.228	1.226	1.275	1.275
C21−Ca1	4.635	4.687	3.564	3.527	2.677	2.681
C21−O19	2.583	2.657	2.605	2.603	1.276	1.273
Ca1−O15	2.339	2.339	2.323	2.321	2.354	2.347
Ca1−O18	2.393	2.455	2.354	2.410	2.333	2.389
Ca1−O14	2.546	2.534	2.572	2.552	2.755	2.663
Al6−O8	1.744	1.782	1.745	1.785	1.745	1.785
Al6−O9	1.744	1.778	1.745	1.778	1.745	1.778
Al12−O18	1.763	1.793	1.764	1.796	1.760	1.819
Al12−O15	1.780	1.814	1.787	1.821	1.785	1.795
Si4−O8	1.612	1.625	1.617	1.629	1.620	1.632
Si5−O9	1.601	1.621	1.601	1.622	1.598	1.619
Si13−O18	1.592	1.608	1.595	1.612	1.596	1.612
Si11−O15	1.611	1.628	1.617	1.634	1.616	1.632
Ca2−C21−O22	162.1	161.3	141.8	140.7	61.6	60.6
O20−Ca2−O19	40.0	40.2	38.8	38.5	29.3	29.2
O20−Ca1−O19	40.1	40.3	46.9	47.0	57.8	58.1
Al6−O8−Si4	130.6	131.2	129.4	130.1	129.3	129.6
Al6−O9−Si5	135.1	134.4	135.7	135.2	136.7	136.4
Ca1−O20−O19−Ca2	119.1	124.6	119.8	124.7	130.6	139.3

Atomic labels are shown in Figure 4.

difference however appears relative to the nonequivalent Ca cationic positions in all Ca_2O_X(6R+4R) clusters. The favored CO location at the upper Ca cation is accompanied by an energy gain around of 6.2 and 5.7 kcal/mol for $X = 2$ and 3, respectively. The same effect of different mono or bidentate CO_2 chemisorption appears in FAU between the products of the CO oxidation over the Ca_2O_2(6R+4R) and Ca_2O_3(6R+4R) moieties (Fig. 5). The higher heat of reaction for $X = 2$ is also assigned to the bidentate CO_2 chemisorption ($\Delta E_{CO2} = 72.6$ kcal/mol, Fig. 5c) versus the monodentate one ($\Delta E_{CO2} = 24.1$ kcal/mol, Fig. 5f), respectively (Table 7). Vibration coordinates for the TS calculated with B3LYP/LANL2DZ(Ca)/6-31G*(Al, Si, O, H) correspond to the vibrations of CO and one O atom with imaginary frequencies of 668.1*i* and 802.2*i* cm^{-1} for $X = 2$ (Fig. 5b) and 3 (Fig. 5e), respectively. This motion is also characterized by a large reduced mass, i.e., 14 a.m.u., versus other imaginary frequencies with smaller reduced masses. However, from 4 to 6 imaginary frequencies only were observed for Ca_2O_X(6R+4R), $X = 2$ or 3, versus 15 or 16 modes for the Ca_2O_X(8R) cluster. We remind that capping H atoms were fixed in the second step of optimization of the isolated cluster. The smaller number of imaginary frequencies of the isolated Ca_2O_X(6R+4R) cluster suggests a less important perturbation of the initially optimized T—H lengths in the course of the optimization as compared to the one for Ca_2O_X(8R). The vibration coordinates for the TS when $X = 3$ are very similar with the B3LYP, B3P86, and PW91PW91 functionals and 6-31G* basis set, even if the frequencies differ substantially, i.e., 833.3*i*, 792.9*i*, and 961.6*i* cm^{-1}, respectively (Table 7).

Discussion

On the basis of the data given earlier, it is a complicated task to choose between the MOR and the FAU type as the most appro-

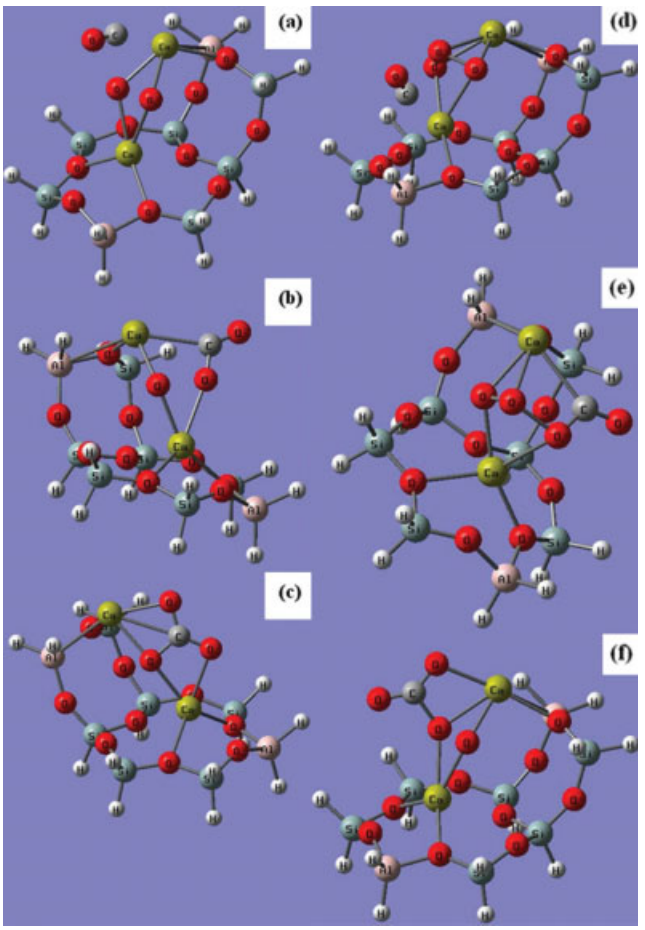

Figure 5. Optimized structures of the reagent (a, d), transition state (b, e), and product clusters (c, f) for CO oxidation over the small Ca_2O_X(6R+4R) clusters in FAU calculated at the B3LYP/6-31G* level, for $X = 2$ (a–c) and $X = 3$ (d–f). The color code corresponds to the one of Figure 3. [Color figure can be viewed in the online issue, which is available at www.interscience.wiley.com.]

Table 7. $\Delta E^{\#}$ Activation Barriers of the Ca_2O_X(6R+4R) + CO → Ca_2CO_{X+1}(6R+4R) Oxidation Reaction, Imaginary Frequencies ω, ΔE_{CO} Heat of CO Adsorption, ΔU Heat of Oxidation Reaction, and ΔE_{CO2} Heat of CO_2 Adsorption, on Ca_2O_X(6R+4R) Clusters of FAU Calculated at the B3LYP/6-31G* Level.

Values	$X = 2$	$X = 3$
$\Delta E^{\#}$	36.4[a]	34.2[a]
$i\omega$	−756.4	−833.3, −792.9[b], −961.6[c]
ΔE_{CO}	15.2	13.6
ΔU	101.4	72.4
ΔE_{CO2}	72.6	24.1

All energy values are in kcal/mol, frequencies are in cm^{-1}.
[a]Related to CO molecule adsorbed at the upper Ca cation.
[b]B3P86.
[c]PW91PW91.

priate zeolite for CO oxidation. On the one hand, both the activation barriers and heats of CO oxidation for MOR and FAU (or Y) are pretty close for $X = 2$ or 3, i.e., the activation barriers nearly coincide within 1–2 kcal/mol. On the other hand, the main problem to compare the calculated characteristics of CO oxidation comes from the absence of experimental data for CO oxidation with both studied forms. Only relative yields of singlet O_2 upon thermal and photothermal stimulations were evaluated for the ZnMOR and ZnY forms.[1] Singlet O_2 desorption from FAU or Y usually happens under slightly low temperatures, i.e., 335 and 329 K versus 342 and 334 K from MOR in air and He flow, respectively. It shows the higher stability of ZnMOR as compared to the one of ZnY. For the Ca-forms, a higher stability of CaY versus CaMOR is noted from the computed heats of the oxidation by molecular oxygen for all the Ca_2O_X(6R+4R) moieties ($X = 1$–3) (Table 1), i.e., the energy gain rises with X from 1.7 (between −26.5 and −24.8 kcal/mol) to 2.5 (between −8.6 and −6.1 kcal/mol) and to 6.9 kcal/mol (between −1.7 and 5.2 kcal/mol). This qualitative growth suggests an opposite higher stability of CaY versus CaMOR. Surely, such a comparison is not complete and requires more experimental data. We should again here emphasize the conclusion of the ref. 2 about the small gas concentration of singlet O_2, i.e., 10^{13} molecule/cm^3. It suggests that singlet O_2 participates as a part of the catalytic sites in the zeolite frameworks (Singlet Dioxygen section) and is not in the gas state.

An additional tip is the relative oxidation activity of ZnY and CaY forms relative to propylene.[1] Together with the main CO and CO_2 products, a small amount of acetic acid appears, which confirms the typical oxidation of double bond in propylene by singlet dioxygen resulting in shortening of carbon chain.[30] The authors from ref. 1 concluded on a higher yield for the CaY form at temperatures above 523 K, while ZnY is more active at lower temperatures. The higher yield of acetic acid in ZnMOR versus the one for CaMOR is in agreement with our earlier study where we have calculated a smaller activation barrier for CO oxidation.[14]

Conclusions

New calcium oxide Ca_2O_X ($X = 1$–4) clusters have been observed at the cationic positions of MOR and FAU zeolites using DFT calculations via the isolated cluster approach. The cationic positions correspond to 8-membered ring (8R) window in MOR and two 6R and 4R windows (6R+4R) possessing one common Si—O—Si side in FAU. Minor differences were observed between the geometries of the Ca_2O_X(8R) and Ca_2O_X(6R+4R) clusters versus X despite the similar bonding in Ca_2O_X(8R) compared to their different bonding of Ca cations to the framework in Ca_2O_X(6R+4R). This invariance is in line with the experimentally observed similar oxidation activities of both alkaline earth MOR and FAU forms.

Close values of the activation energies for CO oxidation over Ca_2O_X(8R) in MOR and Ca_2O_X(6R+4R) in FAU ($X = 2$–3) were demonstrated, i.e., around 30 kcal/mol. The larger heat of CO oxidation over Ca_2O_2(nR) is assigned to the formation of a bidentate CO_3^{2-} anion whose close coordination to the framework is hindered in Ca_2O_3(nR). Earlier in ref. 14, we demonstrated that a partly coordinated CO_2 product over Zn_2O_2(8R) also results in a smaller heat of CO oxidation. The estimations were validated by very similar values of both heat of CO oxidation and activation energies over the considered extended Ca_2O_2(8R) cluster.

The most stable ground states of all the Ca_2O_X(nR) clusters were singlet, which allows to consider these fragments as the source of singlet molecular dioxygen. The yield of singlet O_2 is well documented experimentally with alkaline earth zeolites under elevated temperatures or photo initiation. However, the structure in which singlet O_2 could be accumulated and kept in zeolites has, to our knowledge, not yet been proposed. We, hence, believe that this work could help essentially both to the understanding of the behavior of singlet molecular O_2, on one side, and to give a more complete picture of oxidation over alkaline earth zeolite forms, on the other side. The Ca_2O_2(nR) and Ca_2O_3(nR) clusters can be the most probable sources of singlet O_2 observed experimentally.

References

1. Udalova, O. V.; Khaula, E. V.; Bykhovski, M. Y.; Rufov, Y. N.; Romanov, A. N. Russ J Phys Chem 2003, 77, 912 (transl. from Zurn Fiz Khim 2003, 77, 1018).
2. Udalova, O. V.; Khaula, E. V.; Rufov, Y. N.; Russ J Phys Chem A 2007, 81, 1511 (transl. from Zurn Fiz Khim 2007, 81, 1697).
3. Blatter, F.; Frei, H. J Am Chem Soc 1993, 115, 7501.
4. Blatter, F.; Moreau, F.; Frei, H. J Phys Chem 1994, 98, 13403.
5. Blatter, F.; Frei, H. J Am Chem Soc 1994, 116, 1812.
6. Sun, H.; Blatter, F.; Frei, H. J Am Chem Soc 1994, 116, 7951.
7. Sun, H.; Blatter, F.; Frei, H. J Am Chem Soc 1996, 118, 6873.
8. Panov, A. G.; Larsen, R. G.; Totah, N. I.; Larsen, S. C.; Grassian, V. H. J Phys Chem B 2000, 104, 5706.
9. Larsen, R. G.; Saladino, A. C.; Hunt, T. A.; Mann, J. E.; Xu, M.; Grassian, V. H.; Larsen, S. C. J Catal 2001, 204, 440.
10. Xu, J.; Mojet, B. L.; van Ommen, J. G.; Lefferts, L. J Phys Chem B 2005, 109, 18361.
11. Bregadze, T. A.; Seleznev, V. A.; Kadushin, A. A.; Krylov, O. V. Izv Akad Nauk SSSR Ser Khim 1973, 2701.

12. Patöw, H.; Riekert, L. Ber Bunsenges Phys Chem 1979, 83, 807.
13. Förster, H.; Frede, W.; Peters, G.; Schumann, M.; Witten, U. J Chem Soc Chem Commun 1981, 1064.
14. Zhidomirov, G. M.; Larin, A. V.; Trubnikov, D. N.; Vercauteren, D. P. J Phys Chem C 2009, 113, 8258.
15. Yuan, S.; Wang, J.; Li, Y.; Peng, S. J Mol Catal A 2001, 175, 131.
16. Gale, J. D. GULP 1.3, Royal Institution/Imperial College, UK, 1992/1994.
17. Schröder, K. P.; Sauer, J.; Leslie, M.; Catlow, C. R. A.; Thomas, J. M. Chem Phys Lett 1992, 188, 320.
18. Gale, J. D.; Henson, N. J. J Chem Soc Faraday Trans 1994, 90, 3175.
19. Frisch, M. J.; Trucks, G. W.; Schlegel, H. B.; Scuseria, G. E.; Robb, M. A.; Cheeseman, J. R.; Montgomery, J. A., Jr.; Vreven, T.; Kudin, K. N.; Burant, J. C.; Millam, J. M.; Iyengar, S. S.; Tomasi, J.; Barone, V.; Mennucci, B.; Cossi, M.; Scalmani, G.; Rega, N.; Petersson, G. A.; Nakatsuji, H.; Hada, M.; Ehara, M.; Toyota, K.; Fukuda, R.; Hasegawa, J.; Ishida, M.; Nakajima, T.; Honda, Y.; Kitao, O.; Nakai, H.; Klene, M.; Li, X.; Knox, J. E.; Hratchian, H. P.; Cross, J. B.; Bakken, V.; Adamo, C.; Jaramillo, J.; Gomperts, R.; Stratmann, R. E.; Yazyev, O.; Austin, A. J.; Cammi, R.; Pomelli, C.; Ochterski, J. W.; Ayala, P. Y.; Morokuma, K.; Voth, G. A.; Salvador, P.; Dannenberg, J. J.; Zakrzewski, V. G.; Dapprich, S.; Daniels, A. D.; Strain, M. C.; Farkas, O.; Malick, D. K.; Rabuck, A. D.; Raghavachari, K.; Foresman, J. B.; Ortiz, J. V.; Cui, Q.; Baboul, A. G.; Clifford, S.; Cioslowski, J.; Stefanov, B. B.; Liu, G.; Liashenko, A.; Piskorz, P.; Komaromi, I.; Martin, R. L.; Fox, D. J.; Keith, T.; Al-Laham, M. A.; Peng, C. Y.; Nanayakkara, A.; Challacombe, M.; Gill, P. M. W.; Johnson, B.; Chen, W.; Wong, M. W.; Gonzalez, C.; Pople, J. A. Gaussian 03, Revision C.02. Gaussian, Inc.: Wallingford, CT, 2004.
20. Uytterhoeven, L.; Dompas, D.; Mortier, W. J. J Chem Soc Faraday Trans 1992, 88, 2753.
21. Baur, W. H. Am Mineral 1964, 49, 697.
22. Boddenberg, B.; Seidel, A. J Chem Soc Faraday Trans 1 1994, 90, 1345.
23. Förster, H.; Schumann, M. J Chem Soc Faraday Trans 1 1989, 85, 1149.
24. Huber, K. P.; Herzberg, G. Molecular Spectra and Molecular Structure, Vol. 4:Constants of Diatomic Molecules; Van Nostrand: New York, 1979.
25. Shannon, R. D. Acta Crystallogr A 1976, 32, 751.
26. Carpenter, J. E.; Weinhold, F. J Mol Struct (THEOCHEM) 1988, 46, 41.
27. Larin, A. V.; Vercauteren, D. P. Int J Quantum Chem 2001, 83, 70.
28. Larin, A. V.; Parbuzin, V. S.; Vercauteren, D. P. Int J Quantum Chem 2005, 101, 807.
29. Rozanska, X.; Demuth, T.; Hutschka, F.; Hafner, J.; van Santen, R. A. J Phys Chem B 2002, 106, 3248.
30. Smith, M. B.; March, J. March's Advanced Organic Chemistry, 5th ed.; Wiley: New York, 2001; p 1055.